Journal of Alloys and Compounds 509 (2011) 1222–1225

Contents lists available at ScienceDirect

Journal of Alloys and Compounds

journal homepage: www.elsevier.com/locate/jallcom

Structural and optical analysis of ZnBeMgO powder and thin films

Neeraj Panwar*, J. Liriano, Ram S. Katiyar*

Department of Physics, University of Puerto Rico, San Juan, PR 00931, USA

ARTICLE INFO

Article history:
Received 12 July 2010
Received in revised form
27 September 2010
Accepted 29 September 2010
Available online 8 October 2010

Keywords:
Zinc oxide
Raman studies
Optical UV measurement

ABSTRACT

We here report the structural and optical studies of $Zn_{1-x-y}Be_xMg_yO$ ($0 \le x \le 0.15$; $0 \le y \le 0.20$) powders and thin films. From the Rietveld refinement of the powder X-ray diffraction (XRD) patterns it was revealed that the value of '*a*' lattice parameter remains almost unchanged whereas '*c*' parameter reduces with Be and Mg co-doping in ZnO. The Zn-O bond length also decreases in co-doped samples. Raman studies of the pure ZnO powder showed all the characteristic peaks of the wurtzite hexagonal structure and with (Be, Mg) co-doping new modes appeared which can be attributed to arise as a result of substitution. The XRD of the films prepared from the powders using pulsed laser deposition (PLD) technique exhibited the preferential orientation and with increase in co-doping the (0 0 0 2) peak also shifts to higher 2θ values suggesting the incorporation of Be/Mg at the Zn-site. From the UV–visible optical transmittance measurement it was noticed that the band gap of the pristine ZnO film is 3.3 eV which enhanced up to 4.51 eV for $Zn_{0.7}Be_{0.1}Mg_{0.2}O$ film which lies in the solar blind region and is very useful in the realization of deep UV detectors.

1. Introduction

ZnO is a wide bandgap semiconductor with energy band gap of 3.37 eV and high excitation binding energy (60 meV) at room temperature which makes its versatile for potential applications in many areas like flame detection, missile plume sensing, air quality monitoring, piezoelectric and ferroelectric usage, accurate measurement of radiation for the treatment of UV irradiated skin, ozone hole detection and space-to-space transmission [1–11]. During this decade, the band gap modulation of ZnO films has been achieved by alloying it with much wider band gap semiconductor MgO (7.8 eV) [12–20]. Our group reported the fabrication of stable wide-band gap (~6 eV) ZnO/MgO multilayer thin films using pulsed laser deposition (PLD) technique on *c*-axis oriented sapphire substrate [21]. Ju et al. [22] reported the fabrication of cubic photodetector covering the whole solar blind range (200–280 nm) in cubic $Zn_{1-x}Mg_xO$ ($0.50 \le x \le 0.70$) thin films prepared by metalorganic chemical vapour deposition (MOCVD) technique. However, still there is no stable single-phase wurtzite ZnMgO film with bandgap lying in the solar-blind region (above 4.5 eV). Moreover, there exists a miscibility gap in the ZnO–MgO binary system due to the structural difference and the large lattice mismatch between ZnO (hexagonal wurtzite, 3.25 Å) and MgO (cubic rock salt, 4.22 Å) [12]. Mg^{2+} ions (0.57 Å) can replace 33 at.% of Zn^{2+} ions without changing the structure of ZnO whereas phase segregation between hexagonal ZnO and cubic MgO was observed in $Zn_{1-x}Mg_xO$ alloy with more than 36 at.% Mg-content [12,15–17]. Therefore, the attention shifted towards another binary system ZnBeO [23,24]. BeO possesses the similar wurtzite hexagonal structure of ZnO and a much wider bandgap of 10.8 eV. The electronic structure calculation of ZnBeO by Ding et al. [25] using numeric simulations revealed that the bowing parameter of ZnBeO was greater than GaAlN due to the larger ionic size difference between Be^{2+} (0.27 Å) and Zn^{2+} (0.60 Å) ions. This results in the noticeable lattice mismatch when large bandgap offset between ZnBeO and ZnO is required. Hence the quality of ZnBeO degraded when Be content was increased. In order to obtain high quality crystalline ZnO films with bandgap modulated to solar blind region, incorporation of Be into ZnMgO matrix has been suggested [26]. The large lattice mismatches of ZnO/BeO and ZnO/MgO were expected to be counteracted by each other. Yang et al. [26] deposited ZnBeMgO films on *c*-axis oriented sapphire substrates by pulsed laser deposition (PLD) and increased the bandgap from 3.7 eV to 4.9 eV with the incorporation of different amount of Be and Mg into ZnO matrix. In other study, they also fabricated n-type ZnBeMgO film on p-type silicon substrate and obtained a solar-blind photodetector [27]. The spectral response characteristic with a cutoff wavelength of 280 nm was demonstrated to realize the photodetection of solar-blind region. The photoresponsivity of the film was further enhanced by inserting an Al-doped ZnO (AZO) contact layer. Effect of oxygen partial pressure on structural and optical properties of ZnBeMgO films by pulsed laser deposition has also been recently studied and it was shown that the structure of ZnBeMgO films changed from cubic

* Corresponding authors. Tel.: +1 787 751 4210; fax: +1 787 764 2571.
E-mail addresses: neeraj.panwar@gmail.com (N. Panwar), rkatiyar@uprrp.edu (R.S. Katiyar).

0925-8388/$ – see front matter © 2010 Elsevier B.V. All rights reserved.
doi:10.1016/j.jallcom.2010.09.193

Table 1
Refined parameters of ZnBeMgO powders.

	ZnO	$Zn_{0.85}Be_{0.05}Mg_{0.1}O$	$Zn_{0.80}Be_{0.1}Mg_{0.1}O$	$Zn_{0.75}Be_{0.15}Mg_{0.1}O$	$Zn_{0.70}Be_{0.1}Mg_{0.2}O$
Lattice parameters					
a(Å)	3.251(4)	3.250(4)	3.250(4)	3.250(4)	3.249(4)
c(Å)	5.204(4)	5.186(4)	5.185(4)	5.184(4)	5.183(4)
Zn					
X	0.33330	0.33330	0.33330	0.33330	0.33330
Y	0.66666	0.66666	0.66666	0.66666	0.66666
Z	0.01105	0.00231	0.00231	0.00682	0.00682
Be					
X	–	0.33330	0.33330	0.33330	0.33330
Y	–	0.66666	0.66666	0.66666	0.66666
Z	–	0.00231	0.00231	0.00682	0.00682
Mg					
X	–	0.33330	0.33330	0.33330	0.33330
Y	–	0.66666	0.66666	0.66666	0.66666
Z	–	0.00231	0.00231	0.00682	0.00682
O					
X	0.33330	0.33330	0.33330	0.33330	0.33330
Y	0.66667	0.66667	0.66667	0.66667	0.66667
Z	0.36812	0.37811	0.37811	0.37811	0.37811
χ	1.01	1.18	1.40	1.25	1.50
$\mathbf{R_P}$	11.2	15.1	16.2	15.8	18.0
$\mathbf{R_W}$	18.8	23.2	24.2	24.0	26.7
Phase (%)	100	98.27	95.75	91.78	91.58

rock-salt to hexagonal wurtzite and the bandgap decreased from 4.71 to 4.50 eV with oxygen partial pressure changing from 2×10^{-4} to 2 Pa [28].

Up to now, however, there is no report that shows systematic band gap variation in the ZnO film with different Be and Mg co-doping and synthesized from single targets only (e.g. Yang et al. [27] deposited ZnBeMgO films using ZnMgO and BeO targets). Therefore, we have tried to synthesize ZnBeMgO targets and thin films and report their structural (including XRD and Raman spectrum) and optical properties.

2. Experimental

$Zn_{1-x-y}Be_xMg_yO$ ($0 \le x, y \le 0.10$) powders were synthesized by low energy ball milling. The starting materials used were commercial ZnO (99.99%), BeO (99.5%) and MgO (99.99%) procured from Alfa Aesar. The weighed powders were milled in a solution of propanol with a speed of 90 rpm for 24 h to get homogenization. The solutions thus obtained were heated to evaporate the organic solvents. The dried powders were crushed and calcined at 800 °C for 4 h. The calcined powders were again ground and the pellets were made and heat treated at 600 °C for 2 h, finally sintered at 1100 °C for 4 h. The sintered samples were characterized for XRD with Siemens diffractometer using Cu Kα radiation operated at 40 kV and 40 mA. High quality thin films were grown on (0 0 0 1) oriented Al_2O_3 substrate by pulse laser deposition (PLD) technique using an excimer laser (KrF, 248 nm, 10 Hz repetition frequency) with laser energy of 2.5 J/cm^2. The substrate temperature was maintained at 650 °C. Deposition was done under oxygen pressure of 2–15 mTorr, yielding films of about 0.3 μm thickness. The Raman scattering studies were performed by using Jobin-Yvon T64000 Triple-mate instrument. The radiation of 514.5 nm from Ar^+ laser was used for excitation to perform Raman measurement in backscattering unpolarized mode.

3. Results and discussion

Fig. 1 shows the X-ray diffraction pattern of powder samples. In Pure ZnO all the diffraction peaks corresponding to the wurtzite hexagonal are observed whereas in the co-doped samples reflections corresponding to BeO and MgO can also be identified whose intensity increases with increasing Be and Mg contents. In order to obtain microstructure information of the samples in detail, structure refinement was performed by the Rietveld method using FULLPROOF program. In the refining process, wurtzite ZnO structure was selected as the starting model structure. Be and Mg ions were assumed to incorporate into the ZnO lattice and occupy the Zn^{2+} cites. The refined instrumental and structural parameters were peak shape (using a pseudo-Voigt peak profile function), scale factor, background, unit cell parameters and position coordinates parameters. The structure parameters and R factor values are given in Table 1. Compared with the lattice parameters of pure target, in the doped samples *a* value remains almost unchanged whereas *c* parameter reduces significantly. The lattice volume also decreases and peak shifts slightly to higher 2θ values. This can be understood from the fact that Be^{2+} has much smaller size than Zn^{2+} whereas Mg^{2+} and Zn^{2+} ions have similar ionic sizes. To see the effect of doping on bond length of Zn–O, bond length (l) has been calculated using the following formula [29]:

$$l = \sqrt{\left(\frac{a^2}{3} + \left(\frac{1}{2} - u\right)^2 c^2\right)}$$

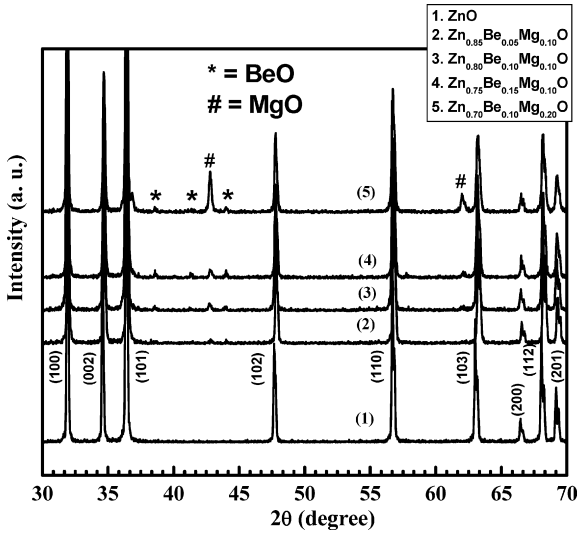

Fig. 1. XRD patterns of $Zn_{1-x-y}Be_xMg_yO$ ($0 \le x \le 0.15$; $0 \le y \le 0.20$) powders.

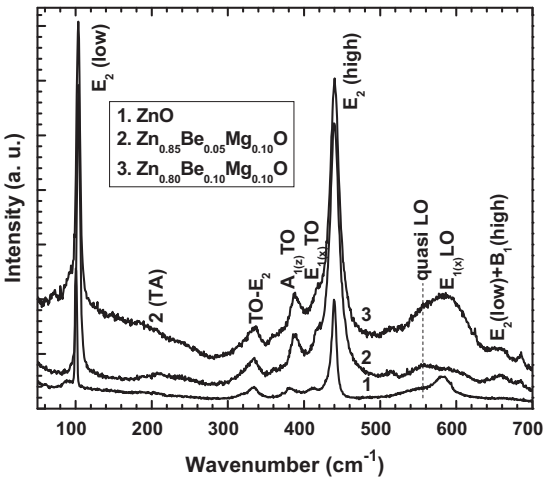

Fig. 2. Room temperature Raman spectra of $Zn_{1-x-y}Be_xMg_yO$ ($0 \le x, y \le 0.10$) powders.

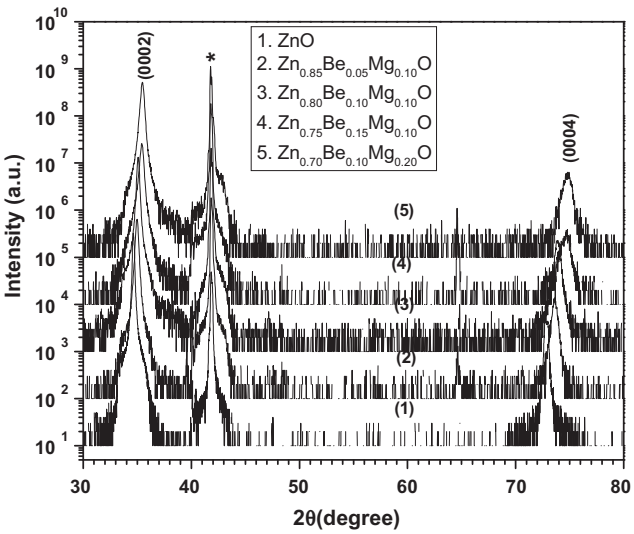

Fig. 3. XRD patterns of $Zn_{1-x-y}Be_xMg_yO$ ($0 \le x \le 0.15$; $0 \le y \le 0.20$) thin films.

where a and c are lattice parameters and u is given by the following relation:

$$u = \frac{a^2}{3c^2} + 0.25$$

It can be observed that the bond length changes from 1.978 Å for pure ZnO to 1.974 Å for $Zn_{0.7}Be_{0.1}Mg_{0.2}O$ sample. From this we can conclude that the bond length decreases because of the smaller ions substitution at the Zn-site.

Now we discuss the Raman studies of the samples up to Be, Mg = 10% co-doping. Raman spectroscopy is a versatile technique to see the effect of dopants on the structural properties of the materials. For ZnO, group theory predicts C_{6v} point group, and there exist 12 degrees of freedom as there are 4 atoms per primitive cell and there are nine optical phonon modes and three acoustic phonon modes [30]. Accordingly, the optical mode at the Γ point can be expressed by $\Gamma_{optic} = A_1 + E_1 + 2E_2 + 2B_1$. The B_1 modes are silent in Raman scattering. A_1 and E_1 modes are polar and split into transverse-optical (TO) and longitudinal-optical (LO) components. Both A_1 and E_1 modes are Raman as well as infrared active. The nonpolar E_2 modes have two frequencies, namely, E_2 (low) and E_2 (high) associated with the motion of zinc (Zn) sublattices and oxygen (O) atoms, respectively [31]. Fig. 2 shows the unpolarized Raman spectra of the samples in backscattered geometry from 50 to 700 cm^{-1}. For the undoped ZnO sample, E_2 optical modes were observed at 100.2 cm^{-1} and 439.4 cm^{-1}. $A_1(z)$(TO), $E_1(x)$(TO), and $E_1(x)$(LO) modes were located at 381 cm^{-1}, 413 cm^{-1}, and 588 cm^{-1}, respectively. High-order Raman peaks were noticed at 208 cm^{-1} (2TA) and 336 cm^{-1} (TO-E_2). The peak positions of the optical phonon modes were in good agreement with the results reported by others [32–35].

In the Be and Mg codoped samples, the E_2 (low) peak is observed at 103.7 cm^{-1} when compared with that for pure ZnO at 100.2 cm^{-1}. E_2 (high) peak shifts from 439.4 cm^{-1} for pure ZnO to 440.0 cm^{-1} for $Zn_{0.8}Be_{0.1}Mg_{0.1}O$ sample. Such shift can be attributed to the smaller size of Be^{2+} than Zn^{2+} (because Mg^{2+} has almost similar ionic size as that of Zn^{2+}, therefore, one cannot expect such shift with Mg^{2+} ion substitution). Also, in comparison to the Raman spectrum of pure ZnO, the additional mode around 556 cm^{-1} in the doped films can be assigned to the quasi-longitudinal-optical (LO) phonon mode, due to the abundant shallow donor defects, such as zinc interstitials (Zn_i) and/or oxygen vacancies (V_O), bounded on the tetrahedral Mg/Be sites. The existence of the quasi-LO phonon mode manifests the incorporation of Mg/Be in the ZnO lattice as its intensity increases with the increase in dopants concentration. Development of such modes with smaller ions doping has been reported earlier also [36–38]. Similarly, the peak intensity of the mode at 685 cm^{-1} also increases with doping and can be thought as an evidence for the incorporation of Be/Mg at Zn-site.

We further present the XRD and optical studies carried out on $Zn_{1-x-y}Be_xMg_yO$ ($0 \le x \le 0.15$; $0 \le y \le 0.20$) thin films deposited from the targets. Fig. 3 shows the XRD patterns (in semi-log scale) of ZnBeMgO films on (0 0 0 1) sapphire substrates. The pristine and the co-doped films exhibit the preferential c-axis orientation indicating that c-axis of the grains become uniformly perpendicular to the substrate surface which can be assigned to the self-texturing mechanism in the films. It is worthwhile to note that, no other phase related to MgO or BeO could be detected in the doped films like those observed in targets. This may be due to the fact that during deposition at lower oxygen pressure some of the Mg^{2+} and Be^{2+} ions (because of their light weights) will be taken out from the plume and will be flushed out of the chamber. In such case there may be lesser ions reaching the substrates. However, in the present case as the targets with higher Be and Mg co-doping possess excess MgO and BeO so during the film growth we get only the single phase film. From the XRD patterns of the films in Fig. 3, it is also clear that the 2θ value of the main peak increases significantly towards higher values. This can be thought due to the incorporation of Be^{2+}/Mg^{2+} – smaller ions at Zn^{2+}-site in ZnO. The full width at half maximum (FWHM) of the pristine ZnO film is 0.18° which gets enhanced up to 0.31° in $Zn_{0.7}Be_{0.1}Mg_{0.2}O$ film. The increase in FHWM reveals that the crystalline nature of the films degrades after the incorporation of Be^{2+}/Mg^{2+} ions because these ions produce distortion in the lattice. The FWHM are comparable to those in Ref. [27].

Fig. 4 shows the transmission spectrum of the films under the same conditions. The films show 80% transmittance in the visible region. No multi-absorption-edge, a typical characteristic of phase separation frequently observed in doped ZnO film, does not occur here. Assuming the absorption coefficient $\alpha \propto -\ln(T)$ corresponding to the direct band gap of the wurtzite structure, a plot of $(\alpha h\upsilon)^2$ versus the photon energy $h\upsilon$ yields in the sharp absorption edge for the high quality thin films by a linear fit. The band gap for the ZnO film is 3.37 eV whereas with 10 Be and 20% Mg co-doped film $Zn_{0.7}Be_{0.1}Mg_{0.2}O$, the band gap increases up to 4.51 eV which lies in the solar blind reason and is helpful in the realization of the deep UV detectors.

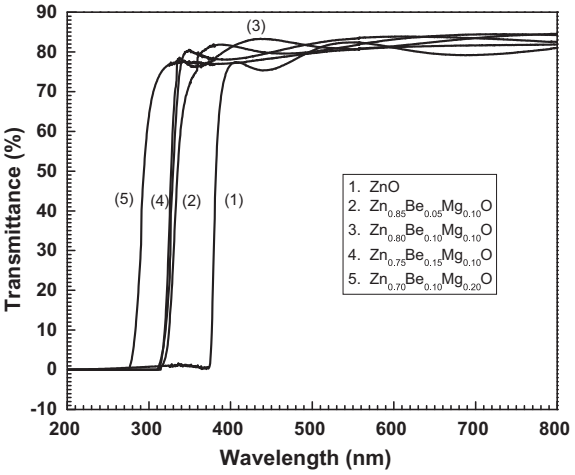

Fig. 4. UV-transmittance spectra of $Zn_{1-x-y}Be_xMg_yO$ ($0 \le x \le 0.15$; $0 \le y \le 0.20$) thin films.

4. Conclusions

Structural (XRD and Raman) and optical properties of $Zn_{1-x-y}Be_xMg_yO$ ($0 \le x \le 0.15$; $0 \le y \le 0.20$) powders and thin films have been studied. XRD analysis of the powders showed that value of '*a*' lattice parameter remains almost same whereas '*c*' parameter reduces with doping. The Zn-O bond also decreases in Be and Mg substituted samples. Raman studies on the pure powder showed all the characteristic peaks of the wurtzite hexagonal structure and with (Be, Mg) co-doping new modes appeared as a result of substitution effect. Thin films fabricated from the powder targets exhibited the preferential orientation and with doping the main (0 0 0 2) peak shifted to higher 2θ values suggesting the incorporation of Be/Mg at the Zn-site. From the UV–visible optical transmittance measurement the calculated band gap of the pristine ZnO film was 3.3 eV and increased to 4.51 eV for $Zn_{0.7}Be_{0.1}Mg_{0.2}O$ film.

Acknowledgement

The authors would like to thank NASA for financial support through grant No. NNX08BA48A.

References

[1] W.L. Hughes, Z.L. Wang, Appl. Phys. Lett. 86 (2005) 043106.
[2] L.E. Greene, M. Law, J. Goldberger, F. Kim, J.C. Johnson, Y. Zhang, R.J. Sakally, P. Wang, Angew. Chem. Int. Ed. 42 (2003) 3031.
[3] T. Abe, Y. Kashiwaba, S. Onodera, F. Masuoka, A. Nakagawa, H. Endo, I. Nikura, Y. Kashiwaba, J. Cryst. Growth 298 (2007) 457.
[4] W. Sang, Y. Fang, J. Fan, Y. He, J. Min, Y. Qian, J. Cryst. Growth 299 (2007) 272.
[5] S.W. Kim, H.K. Park, M.S. Yi, N.M. Park, J.H. Park, S.H. Kim, S.L. Maeng, C.J. Choi, S.E. Moon, Appl. Phys. Lett. 90 (2007) 033107.
[6] M. Ohtsu, K. Kobayashi, T. Kawazoe, S. Sangu, T. Yatsui, IEEE J. Sel. Top. Quantum Electron. 8 (2002) 839.
[7] U. Ozgur, Y.I. Alivov, C. Liu, A. Teke, M.A. Reshchikov, S. Dogan, J. Appl. Phys. 98 (2005) 041301.
[8] X.S. Wang, Z.C. Wu, J.F. Webb, Z.G. Liu, Appl. Phys. A 77 (2003) 561.
[9] K.J. Chen, F.Y. Hung, S.J. Chang, S.J. Young, J. Alloys Compd. 479 (2009) 674.
[10] T. Ghosh, D. Basak, Nanaotechnology 21 (2010) 375202.
[11] N.N. Jandow, F.K. Yam, S.M. Thahab, H.A. Hassan, K. Ibrahim, Curr. Appl. Phys. 10 (2010) 1452.
[12] A. Ohtomo, M. Kawasaki, T. Koida, K. Masubuchi, H. Koinuma, Y. Sakurai, Y. Yoshida, T. Yasuda, Y. Segawa, Appl. Phys. Lett. 72 (1998) 2466.
[13] I. Takeuchi, W. Yang, K.S. Chang, M.A. Aronova, T. Venkatesan, R.D. Vispute, L.A. Bendersky, J. Appl. Phys. 94 (2003) 7336.
[14] S.S. Hullavarad, S. Dhar, B. Varughese, I. Takeuchi, T. Venkatesan, J. Vac. Sci. Technol. A 23 (2005) 982.
[15] X. Zhang, X.M. Li, T.L. Chen, C.Y. Zhang, W.D. Yu, Appl. Phys. Lett. 87 (2005) 092101.
[16] J.F. Kong, W.Z. Shen, Y.W. Zhang, C. Yang, X.M. Li, Appl. Phys. Lett. 92 (2008) 191910.
[17] R. Ghosh, D. Basak, J. Appl. Phys. 101 (2007) 113111.
[18] C. Li, F.Y. Meng, S. Zhang, J.Q. Wang, J. Cryst. Growth 312 (2010) 1929.
[19] K. Yoshino, S. Oyama, M. Yoneta, J. Mater. Sci.: Mater. Electron. 19 (2008) 203.
[20] C.S.S. Sandeep, R. Philip, R. Satheeshkumar, V. Kumar, Appl. Phys. Lett. 89 (2006) 063102.
[21] P. Bhattacharaya, R.R. Das, R.S. Katiyar, Appl. Phys. Lett. 83 (2003) 2010.
[22] Z.G. Ju, C.X. Shan, D.Y. Jiang, J.Y. Zhang, B. Yao, D.X. Zhao, D.Z. Shen, X.W. Fan, Appl. Phys. Lett. 93 (2008) 173505.
[23] Y.R. Ryu, T.S. Lee, J.A. Lubguban, A.B. Corman, H.W. White, J.H. Leem, M.S. Han, Y.S. Park, C.J. Youn, W.J. Kim, Appl. Phys. Lett. 88 (2006) 052103.
[24] W.J. Kim, J.H. Leem, M.S. Han, I.-W. Park, Y.R. Ryu, T.S. Lee, Appl. Phys. Lett. 99 (2006) 096104.
[25] S.F. Ding, G.H. Fan, S.T. Li, K. Chen, B. Xiao, Physica B 394 (2007) 127.
[26] C. Yang, X.M. Li, Y.F. Gu, W.D. Yu, X.D. Gao, Y.W. Zhang, Appl. Phys. Lett. 93 (2008) 112114.
[27] C. Yang, X.M. Li, W.D. Yu, X.D. Gao, X. Cao, Y.Z. Li, J. Phys. D: Appl. Phys. 42 (2009) 152002.
[28] C. Yang, X.M. Li, X.D. Gao, X. Cao, R. Yang, Y.Z. Li, J. Cryst. Growth 312 (2010) 978.
[29] G. Srinivasan, R.T.R. Kumar, J. Sol–Gel Technol. 43 (2007) 171.
[30] D. Shuang, J.B. Wang, X.L. Zhong, H.L. Yan, Mater. Sci. Semicond. Process. 10 (2007) 97.
[31] D.G. Mead, G.R. Wilkinson, J. Raman Spectrosc. 6 (1997) 123.
[32] M.S. Jang, M.K. Ryu, M.H. Yoon, S.H. Lee, H.K. Kim, A. Onodera, S. Kojima, Curr. Appl. Phys. 9 (2009) 651.
[33] C.A. Arguello, D.L. Rousseau, S.P.S. Porto, Phys. Rev. 181 (1969) 1351.
[34] J.M. Calleja, M. Cardona, Phys. Rev. B 16 (1977) 3753.
[35] J. Serrano, A.H. Romeo, F.J. Manjón, R. Lauck, M. Cardona, A. Rubio, Phys. Rev. B 69 (2004) 094306.
[36] T.H. Phan, R. Vincent, D. Cherns, N.X. Nghia, M.H. Phan, S.C. Yu, J. Appl. Phys. 101 (2007) 09H103.
[37] H.K. Yadav, K. Sreenivas, V. Gupta, R.S. Katiyar, J. Appl. Phys. 104 (2008) 053507.
[38] K. Samanta, P. Bhattacharya, R.S. Katiyar, W. Iwamoto, P.G. Pagliuso, C. Rettori, Phys. Rev. B 73 (2006) 245213.